In-Band Scattering from Arrays with Parallel Feed Networks

D. C. Jenn, *Senior Member, IEEE*, and V. Flokas

Abstract—**Approximate closed-form expressions are derived for in-band scattering from an array antenna with parallel (corporate) feed networks. Multiple reflections are neglected and feed devices of the same type are assumed to have identical electrical characteristics. The model is shown to be in good agreement with results generated using a scattering matrix formulation. Based on computed data, the characteristics of array scattering are discussed.**

I. Introduction

SCATTERING from antennas has been the subject of study since the 1950's. Dicke investigated the properties of antenna scattering with the intent of determining the antenna parameters [1]. Extensive work has been done with regard to dipole scattering and the effect of the terminal-load impedance [2], [3]. The radar cross section (RCS) of horns [4], [5], reflector antennas [5], [6], microstrip patches [7], [8], and arrays [9], [10] have also been studied. In most of these works the antenna feed terminals are connected to lumped loads, and only [9] addresses the impact of the feed network on the antenna-scattering pattern.

In this paper, scattering from arrays of elements with parallel (corporate) feed networks is examined. The frequency of the illuminating wave is assumed to be the same as the operating frequency of the array. Therefore, most of the received energy will be delivered to the load at the array terminals if the feed is well designed. However, even for well-matched arrays, small mismatches exist within the feed. For a large array these can number in the thousands. Reflected signals generated at each of the mismatches will return to the aperture and reradiate a scattered field. The total scattered power is a small percentage of the incident power, but the many mismatches can add coherently under some conditions, yielding a significant RCS.

II. Array Radar Cross Section

The prediction of in-band antenna RCS is difficult because of the many scattering sources both at the aperture and in the feed circuit. The basic equation of antenna scattering has been presented by several authors [2], [3], [11]. It gives the total scattered field for a linearly polarized antenna when the antenna port is terminated with a load Z_L

$$\vec{E}^s(Z_L) = \vec{E}^s(Z_a^*) + \left[\frac{j\eta_0}{4\lambda R_a}\vec{h}(\vec{h}\cdot\vec{E}^i)\frac{e^{-jk_0R}}{R}\right]\Gamma_0 \quad (1)$$

where $Z_a = R_a + jX_a$ is the radiation impedance, $\vec{h}$ is the element effective height, and

$$\Gamma_0 = \frac{Z_L - Z_a^*}{Z_L + Z_a^*}. \quad (2)$$

Other quantities in (1) are the wavelength, λ, the impedance of free space, $\eta_0 = 377$ ohms, the free-space wavenumber, $k_0 = 2\pi/\lambda$, and the distance from the target to the observation point, R. Time-harmonic quantities are assumed and the $e^{j\omega t}$ factor suppressed. Traditionally, the antenna scattered field has been decomposed into two components called the structural and antenna (radiation) modes [11]. In (1), $\vec{E}^s(Z_a^*)$ is the structural mode; the second term on the right-hand side is the antenna mode. When the load impedance is the complex conjugate of the radiation impedance, Z_L is called a conjugate-matched load.

Both terms in (1) are small for a well-designed array in its operating band. For a "stand-alone" phased array, such as an array of dipoles over a finite ground plane, the structural mode is primarily due to edge effects—ground plane edge diffraction and mutual coupling changes near the array edges. These affect the scattering at wide angles and for a large array this scattering components is generally small compared to others. For the present analysis, large arrays are assumed and, therefore, only the antenna mode is considered.

For a single element (m,n) in a planar array, as shown in Fig. 1, the monostatic radiation mode is given by

$$\vec{E}^s_{mn}(\theta,\phi) = \left\{\frac{j\eta_0}{4\lambda R_a}\vec{h}[\vec{h}\cdot\vec{E}^i(\theta,\phi)]\frac{e^{-jk_0R}}{R}\right\}\Gamma_{mn}(\theta,\phi) \quad (3)$$

where $\Gamma_{mn}(\theta,\phi)$ represents the total reflected signal returning to aperture element (m,n) when the incident wave is arriving from a direction (θ,ϕ). The effective height can be related to the maximum effective area of an single element [3], and assuming an x-polarized element ($\vec{h} = h\hat{x}$) and a unit magnitude θ-polarized incident plane wave, the θ component of the scattered field becomes

$$(E^s_\theta)_{mn} = \hat{x}\cdot\hat{\theta}\frac{j}{\lambda}A_e\left(e^{-j\vec{k}\cdot\vec{d}_{mn}}\right)\left(\frac{e^{-jk_0r}}{r}\right)\Gamma_{mn}(\theta,\phi). \quad (4)$$

The position vector to element (m,n) is denoted by $\vec{d}_{mn}$ and

$$\vec{k} = k_0(\hat{x}\sin\theta\cos\phi + \hat{y}\sin\theta\sin\phi + \hat{z}\cos\theta).$$

Manuscript received July 11, 1994; revised January 24, 1995.

D. C. Jenn is with the Naval Postgraduate School, Monterey, CA 93943 USA.

V. Flokas is with the Hellenic Navy.

Publisher Item Identifier S 0018-926X(96)01198-2.

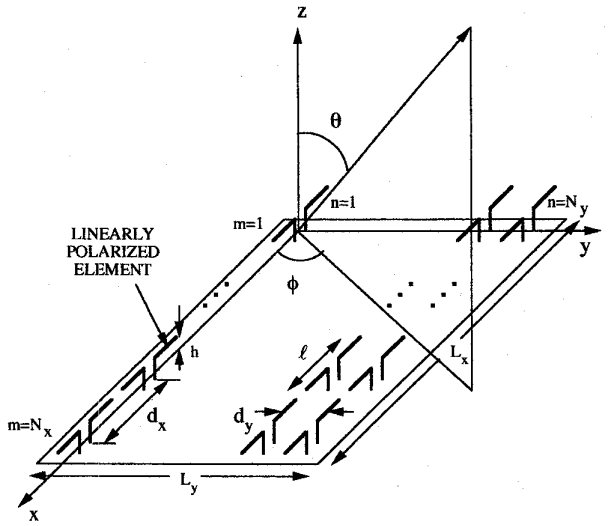

Fig. 1. Planar array geometry.

The effective element area presented to the incident wave is $A_e = \hat{x} \cdot \hat{\theta} A_{em}$. For a large planar array $A_{em} \approx d_x d_y$ so that $A_e \approx \cos\theta \, d_x d_y$.

The total scattered field is obtained by summing over all elements

$$E_\theta^s = \sum_{m=1}^{N_x} \sum_{n=1}^{N_y} (E_\theta^s)_{mn}.$$

Assuming identical elements and using the usual far-field approximations for the scattered wave gives

$$E_\theta^s(r,\theta,\phi) = \left(\frac{jA_e e^{-jk_0 r}}{\lambda r} \right) \sum_{m=1}^{N_x} \sum_{n=1}^{N_y} \Gamma_{mn}(\theta,\phi) e^{j\vec{k}\cdot\vec{d}_{mn}}. \tag{5}$$

Using (5) in the definition of RCS [12] yields

$$\sigma(\theta,\phi) = \frac{4\pi A_e^2}{\lambda^2} \left| \sum_{m=1}^{N_x} \sum_{n=1}^{N_y} \Gamma_{mn}(\theta,\phi) \, e^{j\vec{k}\cdot\vec{d}_{mn}} \right|^2. \tag{6}$$

A diagram of a parallel feed network used to combine the signals from elements lying along the x direction is shown in Fig. 2. Note that the number of elements fed by the network is $N_x = 2^q$ where q is the number of levels of couplers in the feed. The total reflection at the terminals of the elements Γ_{mn} is determined by the impedance seen looking into the feed network. The reflection sources for a typical a parallel feed are labeled in Fig. 2. The first scattering source encountered by the incident wave is the radiating element. If the incident frequency is in the operating band of the array and the wave is arriving at near-normal incidence, the reflection coefficient r_r should be small if the antenna is well designed. The portion of the signal not reflected (t_r) is transmitted into the feed where it proceeds to the phase-shifter input port. If the phase shifter is not exactly matched to the transmission line, a small reflection results. This reflected signal, determined by the reflection

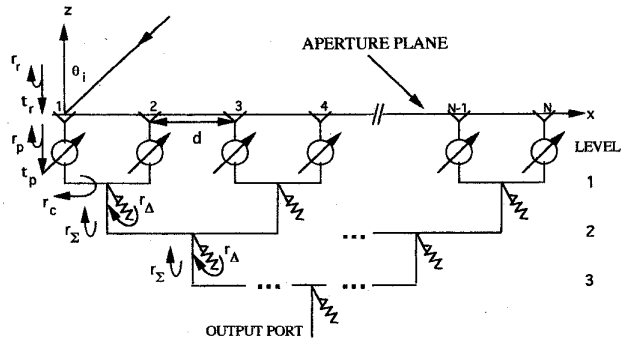

Fig. 2. Parallel feed network.

coefficient r_p, propagates back to the aperture. A portion is again reflected by the radiating element since it is assumed to be reciprocal, and the remainder reradiated. The process continues as the signal travels deeper into the feed network.

An array feed network can be extremely complicated, with potentially every transmission line discontinuity a source of reflected signals. At first glance it might appear that the majority of these reflections are random in phase and amplitude. However, high-performance arrays (i.e., ones with low sidelobes and accurate beam pointing) maintain very close tolerances on phase and amplitude. Consequently, the many small reflected signals inside of the beamformer can add coherently for the same reason that a highly focussed radiation beam is obtained—path lengths to the aperture are designed to provide a linear phase.

It is possible to compute the array RCS rigorously using matrix circuit analysis (e.g., scattering matrices) in conjunction with the method of moments [13]. All interactions between the aperture and devices in the feed network are included, but the formulation is not flexible to changes in the number of elements or type of radiating structure. Furthermore, large amounts of computer memory are required because both the method of moments matrix and the network matrix are solved simultaneously.

The array scattering equations can be reduced to closed form if some assumptions are made with regard to the electrical characteristics of the feed devices. For an approximate analysis of the feed scattering, the following assumptions are made:

1) Devices of the same type have identical electrical characteristics. For example, all the radiating elements have the same reflection and transmission coefficients, r_r and t_r. For convenience, the reflection and transmission coefficient phases of all devices are arbitrarily set to zero. The exception to this is the phase shifter, which has a transmission coefficient of the form

$$t_{p_{mn}} = t_p e^{j\chi_{mn}}$$

where

$$\begin{aligned} \chi_{mn} &= (m-1)\alpha_s + (n-1)\beta_s \\ \alpha_s &= k_0 d_x \sin\theta_s \cos\phi_s \\ \beta_s &= k_0 d_y \sin\theta_s \sin\phi_s. \end{aligned} \tag{7}$$

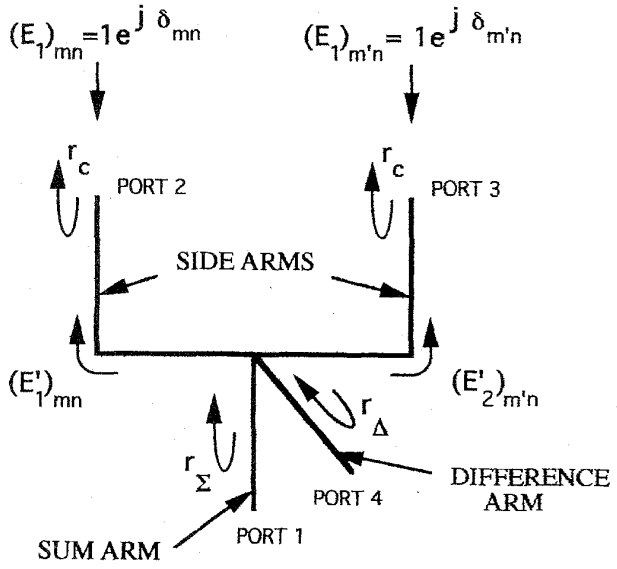

Fig. 3. Magic tee with the difference port loaded.

(θ_s, ϕ_s) is the direction of the array radiation beam. Thus, the magnitude of the transmission coefficient is the same for all phase shifters, but the insertion phase is allowed to vary linearly across the array.

2) All of the couplers are represented by magic tees, which implies uniform excitation of the elements, i.e., this is not a low sidelobe feed.
3) At frequencies in the operating band all of the feed devices are well matched so that $r \ll 1$ and higher order reflections can be neglected.
4) Lossless devices are assumed; for each two-port device $|r|^2 + |t|^2 = 1$.

Now consider an array as shown in Fig. 1 with parallel feed networks along the x direction (the coupling network along the y direction is assumed to be perfectly matched and therefore does not contribute to scattering). With the above limitations, the fraction of the incident signal entering the radiating elements that is reflected at various points in the feed, and then returns to the aperture is given by

$$\Gamma_{mn} \approx r_r e^{j\Delta_{mn}} + t_r^2 r_p e^{j\Delta_{mn}} + t_r^2 t_p^2 r_c e^{j2\chi_{mn}} e^{j\Delta_{mn}} + t_r^2 t_p^2 e^{j\chi_{mn}} [(E_1')_{mn} + (E_2')_{mn} + \cdots] \tag{8}$$

where

$$\begin{aligned} \Delta_{mn} &= (m-1)\alpha + (n-1)\beta \\ \alpha &= k_0 d_x \sin\theta \cos\phi \\ \beta &= k_0 d_y \sin\theta \sin\phi. \end{aligned} \tag{9}$$

The quantities $(E_q')_{mn}$ represent reflected signals returning to element (m, n) which originate at the qth level of couplers. The transmission coefficients are squared because the signal passes through each device twice. The factor of two in the exponent multiplying the coupler terms does not appear explicitly; it is included in the value of $(E_q')_{mn}$.

The RCS is obtained by inserting (8) into (6). The double summation becomes

$$\begin{aligned} &\sum_{m=1}^{N_x} \sum_{n=1}^{N_y} \Gamma_{mn}(\theta, \phi)\, e^{j\vec{k}\cdot\vec{d}_{mn}} \\ &= \sum_{m=1}^{N_x} \sum_{n=1}^{N_y} \left\{ \left(r_r + t_r^2 r_p\right) e^{j2\Delta_{mn}} + t_r^2 t_p^2 e^{j2(\chi_{mn}+\Delta_{mn})} r_c \right. \\ &\qquad \left. + t_c^2 t_r^2 t_p^2 e^{j(\chi_{mn}+\Delta_{mn})} [(E_1')_{mn} + (E_2')_{mn} + \cdots] \right\}. \end{aligned} \tag{10}$$

Now, rearrange (10) so that terms with common reflection coefficients are collected

$$\begin{aligned} &\sum_{m=1}^{N_x} \sum_{n=1}^{N_y} \Gamma_{mn}(\theta, \phi)\, e^{j\vec{k}\cdot\vec{d}_{mn}} \\ &= \sum_{n=1}^{N_y} \left\{ \sum_{m=1}^{N_x} r_r e^{j2\Delta_{mn}} + \sum_{m=1}^{N_x} t_r^2 r_p e^{j2\Delta_{mn}} \right. \\ &\qquad + \sum_{m=1}^{N_x} t_r^2 t_p^2 r_c e^{j2(\Delta_{mn}+\chi_{mn})} + \sum_{m=1}^{N_x} t_r^2 t_p^2 t_c^2 \\ &\qquad \left. \times [(E_1')_{mn} + (E_2')_{mn} + \cdots] e^{j(\Delta_{mn}+\chi_{mn})} \right\}. \end{aligned} \tag{11}$$

The exponentials are separable with respect to the summation indexes m and n. The first three terms are recognized from array theory. Performing the summations gives

$$\begin{aligned} &\sum_{m=1}^{N_x} \sum_{n=1}^{N_y} \Gamma_{mn}(\theta, \phi)\, e^{j\vec{k}\cdot\vec{d}_{mn}} \\ &= \left(r_r + t_r^2 r_p\right) e^{j(N_x-1)\alpha} e^{j(N_y-1)\beta} \frac{\sin(N_x\alpha)}{\sin\alpha} \frac{\sin(N_y\beta)}{\sin\beta} \\ &\quad \cdot t e^{j(N_y-1)(\beta+\beta_s)} \frac{\sin[N_y(\beta+\beta_s)]}{\sin(\beta+\beta_s)} \\ &\quad \times \left\{ t_r^2 t_p^2 r_c e^{j(N_x-1)(\alpha+\alpha_s)} \frac{\sin[N_x(\alpha+\alpha_s)]}{\sin(\alpha+\alpha_s)} + \sum_{m=1}^{N_x} t_r^2 t_p^2 t_c^2 \right. \\ &\qquad \left. \times [(E_1')_{mn} + (E_2')_{mn} + \cdots] e^{j(m-1)(\alpha+\alpha_s)} \right\}. \end{aligned} \tag{12}$$

To evaluate the coupler scattering contribution, expressions for the $(E_q')_{mn}$ must be determined. A magic tee with the difference port loaded is shown in Fig. 3. This configuration can be used to represent any three-port power divider as well. Reflections can arise from mismatches at the inputs of both side arms (r_c at 2 and 3), and the sum and difference output ports (r_Σ at 1 and r_Δ at 4).

Consider a coupler in the first level which combines the received signals from aperture elements m and $m' = m + 1$. The phase angles of the signals delivered to the coupler side

arms are δ_{mn} and $\delta_{m'n}$ where

$$\begin{aligned}\delta_{pn} &= \Delta_{pn} + \chi_{pn} \\ &\equiv (p-1)\xi_x + (n-1)\xi_y \qquad (p = m \text{ or } m') \quad (13)\\ \xi_x &= \alpha + \alpha_s \\ \xi_y &= \beta + \beta_s.\end{aligned}$$

The signal incident on the coupler ($t_r t_p t_c$ in each side arm) is combined in the magic tee according to its scattering matrix

$$\mathbf{C} = \frac{\sqrt{2}}{2}\begin{bmatrix}0 & 1 & 1 & 0\\ 1 & 0 & 0 & 1\\ 1 & 0 & 0 & -1\\ 0 & 1 & -1 & 0\end{bmatrix}. \quad (14)$$

In effect, reflections inside of the magic tee can be modeled by two reflection coefficients: one for the "sum type" of scattering sources (r_Σ) and the other for "difference type" scattering sources (r_Δ). Reflections can originate in the coupling region itself, at the junction of the sum port with the side arm of the next level of couplers, or the difference port load. From a straightforward summation of the incident wave signals and some algebraic manipulation [12], the total reflected signals arriving back at the side arm ports are

$$(E_1')_{mn} = \left[r_\Sigma \cos\left(\frac{\delta_{mn}+\delta_{m'n}}{2}\right) + jr_\Delta \sin\left(\frac{\delta_{mn}+\delta_{m'n}}{2}\right)\right] e^{j(\delta_{mn}+\delta_{m'n})/2} \quad (15)$$

and

$$(E_1')_{m'n} = \left[r_\Sigma \cos\left(\frac{\delta_{mn}+\delta_{m'n}}{2}\right) - jr_\Delta \sin\left(\frac{\delta_{mn}+\delta_{m'n}}{2}\right)\right] e^{j(\delta_{mn}+\delta_{m'n})/2} \quad (16)$$

for $m = 1, 3, 5, \cdots, N_x$. These equations indicate that the RCS is not only dependent on the reflection coefficients, but also on the relative phases of the signals entering the side arms.

The remaining sum in (12) can be reduced to closed form by using (15) and (16). First replace χ_{mn} with its equivalent given in (7) and then substitute in the detailed expressions for $(E_1')_{mn}$ and $(E_1')_{m'n}$. The result is

$$\begin{aligned}&\sum_{m=1}^{N_x}(E_1')_{mn}e^{j(m-1)\xi_x}\\ &= \left[r_\Sigma\cos\left(\frac{\xi_x}{2}\right) + jr_\Delta\sin\left(\frac{\xi_x}{2}\right)\right]\sum_{m=1,3,\ldots}^{N_x} e^{j(4m-3)\xi_x/2}\\ &\quad + \left[r_\Sigma\cos\left(\frac{\xi_x}{2}\right) - jr_\Delta\sin\left(\frac{\xi_x}{2}\right)\right]\\ &\quad \times \sum_{m'=2,4,\ldots}^{N_x} e^{j(4m'-5)\xi_x/2}. \quad (17)\end{aligned}$$

With a change of index and normalization, the sums reduce to

$$\left[r_\Sigma\cos^2\left(\frac{\xi_x}{2}\right)\frac{\sin(N_x\xi_x)}{N_x/2\sin(2\xi_x)} - r_\Delta\sin^2\left(\frac{\xi_x}{2}\right)\frac{\sin(N_x\xi_x)}{N_x/2\sin(2\xi_x)}\right]e^{j(N_x-1)\xi_x}. \quad (18)$$

Thus, (12) has been reduced to a sum of trigonometric functions

$$\begin{aligned}&\frac{1}{N_xN_y}\sum_{m=1}^{N_x}\sum_{n=1}^{N_y}\Gamma_{mn}(\theta,\phi)\,e^{j\vec{k}\cdot\vec{d}_{mn}}\\ &= \left(r_r + r_p t_r^2\right)\frac{\sin(N_x\alpha)}{N_x\sin(\alpha)}\frac{\sin(N_y\beta)}{N_y\sin(\beta)}e^{j(N_y-1)\beta}\\ &\quad\times e^{j(N_x-1)\alpha} + \frac{\sin(N_y\xi_y)}{N_y\sin(\xi_y)}e^{j(N_y-1)\xi_y}\\ &\quad\times\left\{t_r^2t_p^2r_c\frac{\sin(N_x\xi_x)}{\sin(\xi_x)}e^{j(N_x-1)\xi_x} + t_r^2t_p^2t_c^2\right.\\ &\qquad\times\left[r_\Sigma\cos^2\left(\frac{\xi_x}{2}\right) - jr_\Delta\sin^2\left(\frac{\xi_x}{2}\right)\right]\\ &\qquad\left.\times\frac{\sin(N_x\xi_x)}{N_x/2\sin(2\xi_x)}e^{j(N_x-1)\xi_x} + \cdots\right\}. \quad (19)\end{aligned}$$

Equation (19) shows that the total scattered field is a sum of scattering patterns, each one from an identifiable level of the feed

$$E^s = E_r^s + E_p^s + E_c^s + E_{\Sigma_1}^s + E_{\Delta_1}^s + \cdots. \quad (20)$$

If the array size is very large in terms of the incident wavelength, then N_xd_x is large and the pattern functions in (19) have narrow peaks. If this model is to be used to predict the locations of high RCS peaks (usually the case in the initial design stages), then it is sufficient to approximate the magnitude squared of the sum in (20) by the sum of the magnitudes squared

$$\left|E^s\right|^2 \approx \left|E_r^s\right|^2 + \left|E_p^s\right|^2 + \left|E_c^s\right|^2 + \left|E_{\Sigma_1}^s\right|^2 + \left|E_{\Delta_1}^s\right|^2 + \cdots. \quad (21)$$

This neglects the cross products and relative phases of the terms in the scattered field, but allows the total RCS to be expressed as a sum of component radar cross sections

$$\sigma \approx \sigma_r + \sigma_p + \sigma_c + \sigma_{\Sigma_1} + \sigma_{\Delta_1} + \cdots \quad (22)$$

or

$$\begin{aligned}\sigma(\theta,\phi) &= \frac{4\pi A^2\cos^2\theta}{\lambda^2}\\ &\quad\times\left[r_r^2\left(\frac{\sin(N_x\alpha)}{N_x\sin\alpha}\frac{\sin(N_y\beta)}{N_y\sin\beta}\right)^2\right.\\ &\qquad + r_p^2t_r^4\left(\frac{\sin(N_x\alpha)}{N_x\sin\alpha}\frac{\sin(N_y\beta)}{N_y\sin\beta}\right)^2\\ &\qquad + t_r^4t_p^4r_c^2\left(\frac{\sin(N_x\xi_x)}{N_x\sin\xi_x}\frac{\sin(N_y\xi_y)}{N_y\sin\xi_y}\right)^2\\ &\qquad + t_r^4t_p^4t_c^4r_\Sigma^2\cos^4(\xi_x/2)\\ &\qquad\times\left(\frac{\sin(N_x\xi_x)}{N_x/2\sin(2\xi_x)}\frac{\sin(N_y\xi_y)}{N_y/2\sin(2\xi_y)}\right)^2\\ &\qquad + t_r^4t_p^4t_c^4r_\Delta^2\sin^4(\xi_x/2)\\ &\qquad\times\left.\left(\frac{\sin(N_x\xi_x)}{N_x/2\sin(2\xi_x)}\frac{\sin(N_y\xi_y)}{N_y/2\sin(2\xi_y)}\right)^2 + \cdots\right]. \quad (23)\end{aligned}$$

The trigonometric terms in (23) have been normalized by dividing through by N_xN_y and A is the total aperture area of the array, $A = N_xN_yd_xd_y$.

One can extend this result to include more levels of couplers. Two terms must be added to (23) for each additional level of couplers in the feed. One term accounts for sum arm reflections and the second for difference arm reflections. In general, for $q \geq 1$

$$\sigma_{\Sigma_q} = \frac{4\pi A^2 \cos^2\theta}{\lambda^2} t_r^4 t_p^4 t_c^4 r_\Sigma^2 (t_\Sigma)^{2(q-1)} \times \left[\prod_{\ell=1}^{q-1} \cos^4\left(\frac{2^{(\ell-1)}\xi_x}{2}\right)\right] \cos^4\left[2^{(q-1)}\xi_x\right] \times \left(\frac{\sin(N_x\xi_x)}{N_x/2^q \sin(2^q\xi_x)} \frac{\sin(N_y\xi_y)}{N_y \sin(\xi_y)}\right)^2 \quad (24)$$

$$\sigma_{\Delta_q} = \frac{4\pi A^2 \cos^2\theta}{\lambda^2} t_r^4 t_p^4 t_c^4 r_\Delta^2 (t_\Sigma)^{2(q-1)} \times \left[\prod_{\ell=1}^{q-1} \cos^4\left(\frac{2^{(\ell-1)}\xi_x}{2}\right)\right] \sin^4\left[2^{(q-1)}\xi_x\right] \times \left(\frac{\sin(N_x\xi_x)}{N_x/2^q \sin(2^q\xi_x)} \frac{\sin(N_y\xi_y)}{N_y \sin(\xi_y)}\right)^2. \quad (25)$$

The factor $(t_\Sigma)^{2(q-1)}$ accounts for energy lost from reflections at the $q-1$ previous levels of couplers.

III. Computed Data

The validity of the approximate model is demonstated by comparing results obtained using (23) to those from a scattering matrix formulation similar to the one described in [13]. For the scattering matrix solution the aperture element is simply represented by a two-port device with reflection coefficient r_r. This allows direct comparison of the approximate and matrix solutions. Since the element scattering model is the same, any difference can be attributed to the assumptions made in the development of (23).

Consider a phased array antenna operating at wavelength λ_o with the following parameters:

- $N_x = 64$ and $N_y = 1$ (linear array);
- $d_x = 0.5\lambda_o$, $\phi = 0°$, and $h = \lambda_o$ (d_y is replaced by h in (23) to obtain linear array RCS from the planar array formulas);
- $r_r = r_p = r_c = r_\Sigma = r_\Delta = 0.2$ (all reflection coefficients are 0.2);
- incident wave frequency equal to the operating frequency of the antenna ($\lambda = \lambda_o$);
- three levels of couplers ($r_\Sigma = r_\Delta = 0$ for $q > 3$).

The matrix calculation has been limited to three levels of couplers to keep the number of simultaneous equations manageable. With $q = 3$, subarrays of eight elements are coupled at the aperture (i.e., the eight elements sharing the same coupler at the third level). Because all devices of the same type are assumed identical, the matrix solution need only be applied to eight elements. Larger arrays can be decomposed into arrays of eight-element subarrays with the appropriate phase-shifted excitation. In this case, 60 simultaneous equations must be solved.

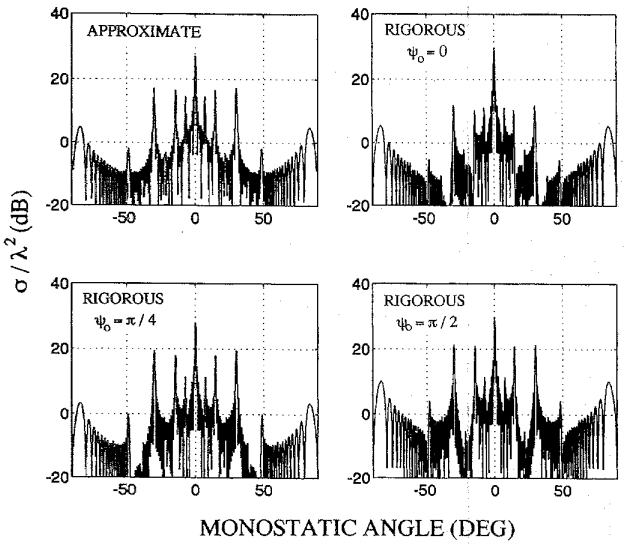

Fig. 4. Comparison of the approximate and matrix solutions for a linear array ($N_x = 64$, $d_x = 0.5\lambda$, $h = 1\lambda$, $\theta_s = \phi_s = 0°$, $\phi = 0°$ and three levels of couplers).

The two solutions are compared in Fig. 4. The highest lobe at $\theta = 0°$ is primarily due to specular scattering from the aperture, although feed reflections also contribute. The lobes near $\theta = \pm 90°$ arise from Bragg diffraction. Spikes between the specular and Bragg lobes are from coupler mismatches. The matrix solution allows specification of the line lengths between devices in the feed. Three patterns in Fig. 4 show the RCS for line lengths of $\psi_0 = 0$, $\pi/4$, and $\pi/2$. As expected, the lobe heights vary with ψ_0 because the phases of the reflected signals change with line length. This effect is not observed in the approximate solution because the noncoherent sum (21) is used in place of (20). Note that (21) is not crucial to the development of the approximate model; it simply allows the total RCS be be written as a sum of radar cross sections.

The behavior of the RCS with scan is illustrated in Fig. 5. If the radiation beam is scanned, then RCS lobes depending on the terms with ξ_x and ξ_y also scan. Fig. 5 shows the RCS obtained for a beam scan of 45° in the x-z plane ($\alpha_s = -kd_x \sin(\pi/4)$). Note that RCS components arising from reflections ahead of the phase shifters remain fixed.

The RCS characteristics of two-dimensional arrays can be visualized by plotting constant level contours in direction cosine space. Fig. 6 shows the RCS of a square planar array with a scanned radiation beam ($\theta_s = 30°$, $\phi_s = 45°$) and the parameters listed above except that $N_y = 64$ and $d_y = 0.5$. High levels are present along the principal planes of the array, but the levels drop off quickly away from these planes because of the separable products in (23). As in the linear array case, the contours originating from reflections behind the phase shifters scan along with the antenna beam. Because the RCS terms are separable in direction cosine space the contours are straight lines (i.e., $u = \sin\theta\cos\phi$ a constant and $v = \sin\theta\sin\phi$ a constant).

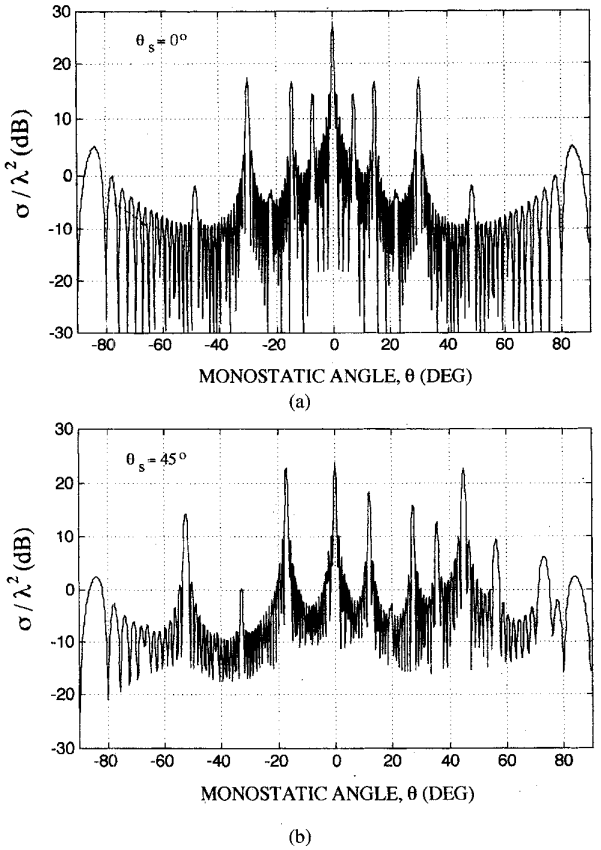

Fig. 5. Monostatic RCS of a linear array ($N_x = 64$, $d_x = 0.5\lambda$, $h = 0.5\lambda$, and three levels of couplers). (a) $\theta_s = 0°$. (b) $\theta_s = 45°$.

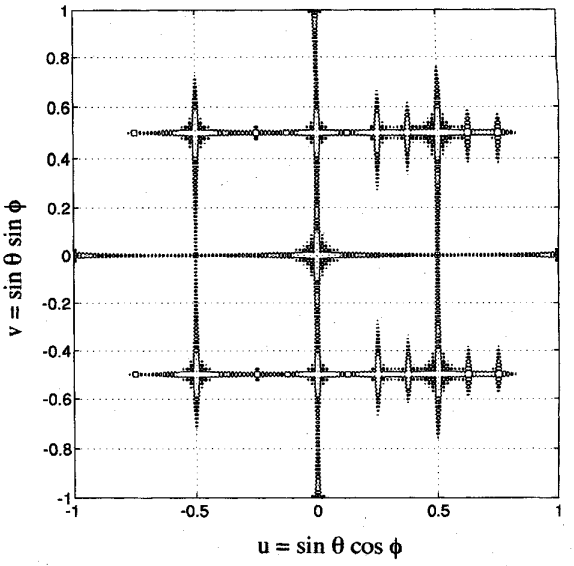

Fig. 6. Monostatic RCS of a planar array for a scanned radiation beam ($N_x = N_y = 64$, $d_x = d_y = 0.5\lambda$, $\theta_s = 30°$, $\phi_s = 45°$, and three levels of couplers). Contours enclose areas of $\sigma/\lambda^2 \geq 20$ dB.

IV. Summary and Discussion

An examination of the computed RCS in the last section reveals several important characteristics:

1) The level of the lobes increases with the magnitudes of the reflection coefficients and the area. The area depends on the number of elements and their spacing.
2) The lobe spacing in the RCS pattern for the first level of couplers is determined by the physical spacing of the couplers, $2d_x$. This holds for other levels of couplers as well. For instance, the second level of couplers are spaced a distance $4d_x$ and therefore a new set of RCS lobes appear between the lobes generated by the first level of couplers.
3) Lobes associated with reflections occuring behind the phase shifters contain the factor χ_{mn} and thus, their positions are determined by the phase shifter settings.

The approximate results degrade gracefully as the assumption of small reflection coefficients is violated. As a typical example, when compared to a rigorous result with $\psi_0 = \pi/4$, the approximate solution peaks were generally within 2 dB for $r = 0.1$, but only 5 dB when $r = 0.4$.

The approximate formulas are conservative, i.e., yield higher than actual RCS peak levels, for several reasons. First, a lossless feed network was assumed. All practical antennas have some loss and feeds with solid-state devices can have significant losses. It is not unusual to encounter phase shifters with 1 to 2 dB of loss, and because the scattered signals travel through the device twice, the net reduction on RCS can be significant (note the t_p^4 dependence for reflections that occur behind the phase shifters). Second, equal power splitters have been assumed. For a low sidelobe antenna the feed is designed to provide a tapered amplitude distribution. The required coupler distribution will also yield some reduction in RCS sidelobes relative to those obtained using equal power splitters. Finally, all reflection coefficients of similar devices will not be the same as postulated. As a result of manufacturing imperfections they have random amplitude and phase components with some mean and variance. The approximate equations derived here can be used to predict the average RCS of the array if average values of transmission and reflection coefficients are used.

References

[1] C. G. Montgomery, R. H. Dicke, and E. M. Purcell, *Principles of Microwave Circuits*. MIT Radiation Lab. Ser., McGraw-Hill, vol. 8, p. 317.
[2] Y. Y. Hu, "Back-scattering cross section of a center-loaded antenna," *IRE Trans. Antennas Propagat.*, vol. AP-6, no. 1, p. 140, Jan. 1958.
[3] D. D. King, "The measurement and interpretation of antenna scattering," *Proc. of the IRE*, vol. 37, no. 7, pp. 770–777, July 1949.
[4] D. Midgley, "A theory of receiving aerials applied to the reradation of an electromagnetic horn," *Proc. of the IEE*, vol. 108, part B, no. 42, pp. 645–650, Nov. 1961.
[5] N. Williams, "The RCS of antennas—An appraisal," in *Military Microwaves Conf. Proc.*, Brighton, U.K., June 1986, pp. 505–508.
[6] D. C. Jenn, J. E. Fletcher, and A. Prata, "Radar cross section of symmetric reflectors with cavity-backed dipole feeds," *IEEE Trans. Antennas Propagat.*, vol. 41, no. 7, pp. 992–994, July 1993.
[7] D. M. Pozar, "Radiation and scattering from a microstrip patch on a uniaxial substrate," *IEEE Trans. Antennas Propagat.*, vol. AP-35, pp. 613–621, June 1987.
[8] E. H. Newman and E. Forrai, "Scattering from a microstrip patch," *IEEE Trans. Antennas Propagat.*, vol. AP-35, pp. 245–251, Mar. 1987.

[9] P. J. Tittensor and M. L. Newton, "Prediction of the radar cross section of an array antenna," in *Sixth Int. Conf. Antennas Propagat.*, London, U.K., Apr. 1989, pp. 258–262.
[10] R.-S. Chu, D. C. Jenn, and N. S. Wong, "Scattering from a finite phased array of dipoles over a finite ground plane," in *1987 IEEE AP-S Int. Symp. Dig.*, June 1987, vol. II, pp. 722–726.
[11] R. C. Hansen, "Relationships between antennas as scatterers and as radiators," in *Proc. IEEE*, vol. 77, no. 5, pp. 659–671, May 1989.
[12] V. Flokas, "In-band radar cross section of phased arrays with parallel feeds," master's thesis, Naval Postgrad. School, June 1994.
[13] D. C. Jenn, "A complete matrix method for antenna analysis," in *1989 IEEE AP-S Int. Symp. Dig.*, June 1989, p. 126.

D. C. Jenn (S'75–A'79–M'82–SM'93), photograph and biography not available at the time of publication.

V. Flokas was born in Athens, Greece, on December 28, 1963. He graduated from the Hellenic Naval Academy in 1985 and received the M.S. degree in electrical engineering from the U.S. Naval Postgraduate School, Monterey, CA, in December 1994.

Since 1985, his shipboard duties with the Hellenic Navy have included Electronics Officer and Engineer.